Steel and Composite Structures, *Vol. 35, No. 1* (*2020*) *111-127*
DOI: https://doi.org/10.12989/scs.2020.35.1.111

Influence of porosity distribution on vibration analysis of GPLs-reinforcement sectorial plate

Anqiang Jia[1,2], Haiyan Liu[3], Lijian Ren[1], Yingxia Yun*[1] and Vahid Tahouneh**[4]

[1]*School of Architecture, Tianjin University, Tianjin 300072, China*
[2]*Institute of Urban and Rural Construction, Hebei Agricultural University, Baoding, Hebei 071001, China*
[3]*College of Sciences, Hebei Agricultural University, Baoding, Hebei 071001, China*
[4]*Young Researchers and Elite Club, Islamshahr Branch, Islamic Azad University, Islamshahr, Iran*

(*Received September 27, 2019, Revised January 11, 2020, Accepted January 12, 2020*)

Abstract. The goal of this study is to fill this apparent gap in the area about investigating the effect of porosity distributions on vibrational behavior of FG sectorial plates resting on a two-parameter elastic foundation. The response of the elastic medium is formulated by the Winkler/Pasternak model. The internal pores and graphene platelets (GPLs) are distributed in the matrix either uniformly or non-uniformly according to three different patterns. The model is proposed with material parameters varying in the thickness of plate to achieve graded distributions in both porosity and nanofillers. The elastic modulus of the nanocomposite is obtained by using Halpin-Tsai micromechanics model. The annular sector plate is assumed to be simply supported in the radial edges while any arbitrary boundary conditions are applied to the other two circular edges including simply supported, clamped and free. The 2-D differential quadrature method as an efficient and accurate numerical approach is used to discretize the governing equations and to implement the boundary conditions. The convergence of the method is demonstrated and to validate the results, comparisons are made between the present results and those reported by well-known references for special cases treated before, have confirmed accuracy and efficiency of the present approach. It is observed that the maximum vibration frequency obtained in the case of symmetric porosity and GPL distribution, while the minimum vibration frequency is obtained using uniform porosity distribution. Results show that for better understanding of mechanical behavior of nanocomposite plates, it is crucial to consider porosities inside the material structure.

Keywords: sectorial plates; vibration; pores and graphene platelets; Halpin-Tsai micromechanics model; elastic foundation

1. Introduction

Normally, Functionally graded materials (FGMs) are heterogeneous materials in which the elastic and thermal properties change from one surface to the other, gradually and continuously. The material is constructed by smoothly changing the volume fraction of its constituent materials. FGMs offer great promise in applications where the operating conditions are severe, including spacecraft heat shields, heat exchanger tubes, plasma facings for fusion reactors, engine components, and high-power electrical contacts or even magnets. For example, in a conventional thermal barrier coating for high-temperature applications, a discrete layer of ceramic material is bonded to a metallic structure. However, the abrupt transition in material properties across the interface between distinct materials can cause large interlaminar stresses and lead to plastic deformation or cracking (Finot and Suresh 1996). These adverse effects can be alleviated by functionally grading the material to have a smooth spatial variation of material composition. The concept of FGMs was first introduced in Japan in 1984. Since then it has gained considerable attention (Koizumi 1993). A lot of different applications of FGMs can be found in (Zhu and Meng 1995). Ramakris and Kunukkas (1973) provided a closed-form analytical solution for free vibration of an annular sector plate with radial edges simply supported. Mukhopadhyay (1979, 1982) used a semi-analytical method and Srinivasan and Thiruvenkatachari (1983, 1986) used the integral equation technique to analyze the vibrations of annular sector plates, respectively. Kim and Dickinson (1989) used one-dimensional (1-D) orthogonal polynomials and Liew and Lam (1993) used two-dimensional (2-D) orthogonal polynomials as admissible functions to study the free vibration of annular sector plates by the Rayleigh–Ritz method. Ramaiah and Vijayakumar (1974) studied the free vibration of annular sector plates with simply supported radial edges by a combination of the Rayleigh-Ritz method and coordinate transformation. Swaminadham *et al*. (1984) compared the natural frequencies of annular sector plates from the finite element method and experiments. Seok and Tiersten (2004) used a variational approximation procedure to analyze the free vibration of cantilevered annular sector plates. Houmat (2001) used the hierarchical finite element method to study the free vibration of annular sector plates. Marin and Marinescu (1998), studied thermoelasticity of

*Corresponding author, Ph.D.
E-mail: jiaanqiang111@163.com
[a] Ph.D.
E-mail: vahid.th1982@gmail.com

ISSN: 1229-9367 (Print), 1598-6223 (Online)

initially stressed bodies. They first wrote the mixed initial boundary value problem within the context of thermoelasticity of initially stressed bodies.

Then they established some Lagrange type identities and also introduced the Cesaro means of various parts of the total energy associated to the solutions. In another study (Marin *et al.* 2017) is dedicated to the Saint-Venant's problem in the context of the theory of porous dipolar bodies. Marin and Craciun (2017) use dipolar elasticity to model composites with microstructure that can display nonlocal effects. A mixed initial boundary problem is addressed for dipolar thermoelasticity. Marin *et al.* (2017) investigate the theory of micropolar thermoelastic bodies whose micro-particles possess microtemperatures. Marin and Lupu (1998) obtained a spatial estimate, similar to that of Saint-Venant type by using a measure of Toupin type associated with the corresponding steady-state vibration and assuming that the exciting frequency was lower to a certain critical frequency. Marin (2010) extended the concept of domain of influence in order to cover the elasticity of microstretch materials. Sharma *et al.* (2005a, b) integrated an analytical approach with the Chebyshev polynomials technique to study the buckling and free vibration of isotropic and laminated composite sector plates based on the first-order shear deformation theory. Liu and Wang (2015) studied Thermal vibration of a single-walled carbon nanotube predicted by semiquantum molecular dynamics. Zhang and Wang (2018) investigated the nonlinear thermal vibrational behavior of single-layered BP (SLBP) via a nonlinear orthotropic plate model (OPM) and molecular dynamics (MD) simulations. Xu *et al.* (2016) studied the vibration of double-layered graphene sheets (DLGS) using A nonlocal Kirchhoff plate model with the van der Waals (vdW) interactions. Ahmed Houari *et al.* (2018) presented a closed-form solutions for exact critical buckling loads of nonlocal strain gradient functionally graded beams. For moderate thickness plates, the first-order shear deformable plate theory is commonly used, which could provide a result more accurate than that from the CPT. Liew and Liu (2000) used the differential quadrature method to analyze the free vibration of thick annular sector plates. Rao *et al*. (1977) and Guruswamy and Yang (1979) used the finite element method to analyze the vibrations of thick annular sector plates. Chen *et al.* (2017) investigated vibration and stability of initially stressed sandwich plates with FGM face sheets. Barka *et al.* (2016) studied thermal post-buckling behavior of imperfect temperature-dependent FG structures. Bouguenina *et al*. (2015) studied FG plates with variable thickness subjected to thermal buckling. Park *et al*. (2016) used modified couple stress based third-order shear deformation theory for dynamic analysis of sigmoid functionally graded materials (S-FGM) plates. Wu and Liu (2016) developed a state space differential reproducing kernel (DRK) method in order to study 3D analysis of FG circular plates. Benson and Hinton (1976) and Cheung and Chan (1981) used the finite strip method to carry out static and dynamic analyses of thick annular sector plates. Mizusawa (1991) used the finite element method to study the natural frequencies of thick annular sector plates. Xiang *et al.* (1993) applied the Ritz method to study the free vibration of thick annular sector plates. Leissa *et al*. (1993 and 1995) considered the effect of stress singularities on the vibration analysis of thick annular sector plates and presented the corner functions to improve the convergence of the numerical solutions. Zhou *et al*. (2009) used the Chebyshev-Ritz method to study the free vibration of thick annular sector plates, Nie and Zhong (2008) investigated the free and forced vibration analysis of FGM annular sector plates with simply-supported radial edges by using a semi-analytical approach. Arefi (2015) suggested an analytical solution of a curved beam with different shapes made of functionally graded materials (FGMs). Bennai *et al*. (2015) developed a new refined hyperbolic shear and normal deformation beam theory to study the free vibration and buckling of functionally graded (FG) sandwich beams under various boundary conditions. Bouchafa *et al.* (2015) used refined hyperbolic shear deformation theory (RHSDT) for the thermoelastic bending analysis of functionally graded sandwich plates. Tahouneh (2016) presented a 3-D elasticity solution for free vibration analysis of continuously graded carbon nanotube-reinforced (CGCNTR) rectangular plates resting on two-parameter elastic foundations. The volume fractions of oriented, straight single-walled carbon nanotubes (SWCNTs) were assumed to be graded in the thickness direction. Moradi-Dastjerdi and Momeni-Khabisi (2016) studied Free and forced vibration of plates reinforced by wavy carbon nanotube (CNT). The plates were resting on Winkler-Pasternak elastic foundation and subjected to periodic or impact loading.

Nowadays, the use of carbon nanotubes in polymer/carbon nanotube composites has attracted wide attention (Wagner *et al.* 1997). A high aspect ratio, low weight of CNTs and their extraordinary mechanical properties (strength and flexibility) provide the ultimate reinforcement for the next generation of extremely lightweight but highly elastic and very strong advanced composite materials. On the other hand, by using of the polymer/CNT composites in advanced composite materials, we can achieve structures with low weight, high strength and high stiffness in many structures of civil, mechanical and space engineering.

Several researches have recently investigated the elastic properties of multiwalled carbon nanotube (MWCNT) and their composites (Fidelus *et al.* 2005, Ghavamian, Rahmandoust and Öchsner 2012). Gojny *et al.* (2005) focused on the evaluation of the different types of the CNTs applied, their influence on the mechanical properties of epoxy-based nanocomposites and the relevance of surface functionalization. Therefore, the study of the mechanical performance of CNT-based composites and the discovery of possible innovative applications has recently attracted the interest of many researchers.

Many researchers have reported that mechanical properties of polymeric matrices can be drastically increased (Montazeri *et al*. 2010, Yeh *et al.* 2006) by adding a few weight percent (wt%) MWCNTs. Montazeri et al. (2010) showed that modified Halpin-Tsai equation with exponential Aspect ratio can be used to model the experimental result of MWNT composite samples. They also demonstrated that reduction in Aspect ratio (L/d) and

nanotube length cause a decrease in aggregation and Above 1.5 wt%, nanotubes agglomerate causing a reduction in Young's modulus values. Thus, it is important to determine the effect Aspect ratio and arrangement of CNTs on the effective properties of carbon nanotube-reinforced composite (CNTRC). Yeh *et al*. (2006) used the Halpin-Tsai equation to shows the effect of MWNT shape factor (L/d) on the mechanical properties. They showed that the mechanical properties of nanocomposite samples with the higher shape factor (L/d) values were better than the ones with the lower shape factor. The reinforcement effect of MWCNTs with different aspect ratio in an epoxy matrix has been carried out by Martone *et al*. (2011). They showed that progressive reduction of the tubes effective aspect ratio occurs because of the increasing connectedness between tubes upon an increase in their concentration. Also they investigated on the effect of nanotube curvature on the average contacts number between tubes by means of the waviness that accounts for the deviation from the straight particles assumption. Tornabene *et al.* (2019) investigated free vibration analysis of arches and beams made of composite materials via a higher-order mathematical formulation. Tornabene *et al*. (2017) studied free vibration analysis of composite sandwich plates and doubly curved shells with variable stiffness. The reinforcing fibers were located in the external skins of the sandwich structures according to curved paths. Tornabene *et al*. (2018) studied free vibration of laminated nanocomposite plates and shells using first-order shear deformation theory and the Generalized Differential Quadrature (GDQ) method. Each layer of the laminate was modelled as a three-phase composite. A survey of several methods under the heading of strong formulation finite element method (SFEM) was presented by Tornabene *et al*. (2015).

The present work aims to investigate the free vibration of FG sectorial plates with GPLs either uniformly or non-uniformly dispersed in the metal matrix. Two non-uniform and the uniform porosity distributions are employed and their performance is compared. A 3-D theory of elasticity is used for theoretical formulations of the nanocomposite plate with porosity coefficients and GPL nanofiller contents varying in the thickness direction. The effects of GPL reinforcing nanofillers and the porosity distribution are studied in detail through a parametric study to find out the best GPL and porosity distributions to achieve the highest effective plate stiffness.

2. Problem description

Consider an annular sector plate resting on two-parameter elastic foundations as shown in Fig. 1. This plate is referring to a cylindrical coordinate system (r,θ,z), as depicted in Fig. 1. It is assumed the thickness of structure is "h". The structure has continuous grading of GPLs-reinforcement through thickness direction. Three different GPL dispersion patterns, denoted by A, B, and C, are considered for each porosity distribution (Fig. 2). The GPL volume content V_{GPL} is assumed to vary along the z-axis smoothly with its peak values (S_{ij}, i,j=1, 2, 3) being determined based on the specific porosity distribution. To facilitate a direct and meaningful comparison, the total amount of GPLs is kept the same for three different GPL distribution patterns. This leads to $s_{1i}\neq s_{2i}\neq s_{3i}$ (i=1, 2, 3).

The mechanical properties of a porous plate with different types of porosity distributions can be expressed by

$$E(z)=E_1(1-e_0\lambda(z)) \tag{1}$$

$$G(z)=E(z)/2(1+\upsilon(z)) \tag{2}$$

$$\rho(z)=\rho_1(1-e_m\lambda(z)) \tag{3}$$

in which, for symmetric porosity distribution

$$\lambda(z)=\cos(\pi z/h) \tag{4}$$

for asymmetric porosity distribution

$$\lambda(z)=\cos(\pi z/2h+\pi/4) \tag{5}$$

and for uniform porosity distribution

$$\lambda(z)=\lambda \tag{6}$$

where E_1, G_1, and ρ_1 are the maximum values of elasticity moduli, shear moduli and mass density.

Also, e_0 and e_m are the coefficients of porosity and mass density, respectively, defined by (Kitipornchai *et al.* 2017)

$$e_0=1-\frac{E_2}{E_1}=1-\frac{G_2}{G_1}$$
$$e_m=\frac{1.121(1-\sqrt[2.3]{1-e_0\lambda(z)})}{\lambda(z)} \tag{7}$$

Also based on the closed-cell graphene-reinforcement scheme, Poisson's ratio (z) can be expressed by (Kitipornchai *et al*. 2017)

$$\upsilon(z)=0.221\tilde{\rho}+\upsilon_1(0.342\tilde{\rho}^2-1.21\tilde{\rho}+1) \tag{8}$$

In which $\boldsymbol{\upsilon}_1$is the Poisson's ratio of pure matrix materials without pores and

$$\tilde{\rho}=1.121(1-\sqrt[2.3]{1-e_0\lambda(z)}) \tag{9}$$

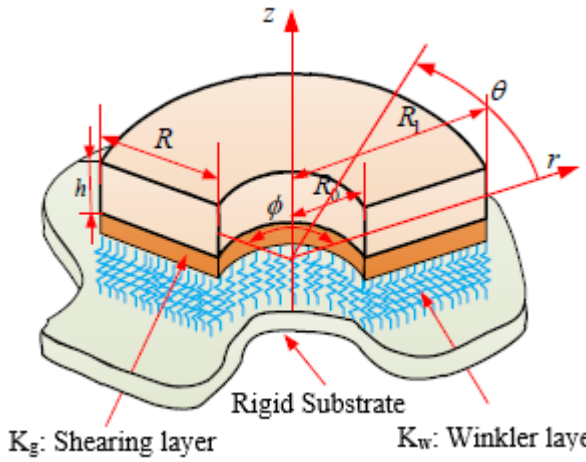

Fig. 1 The sketch of a thick nanocomposite sectorial plate and setup of the coordinate system

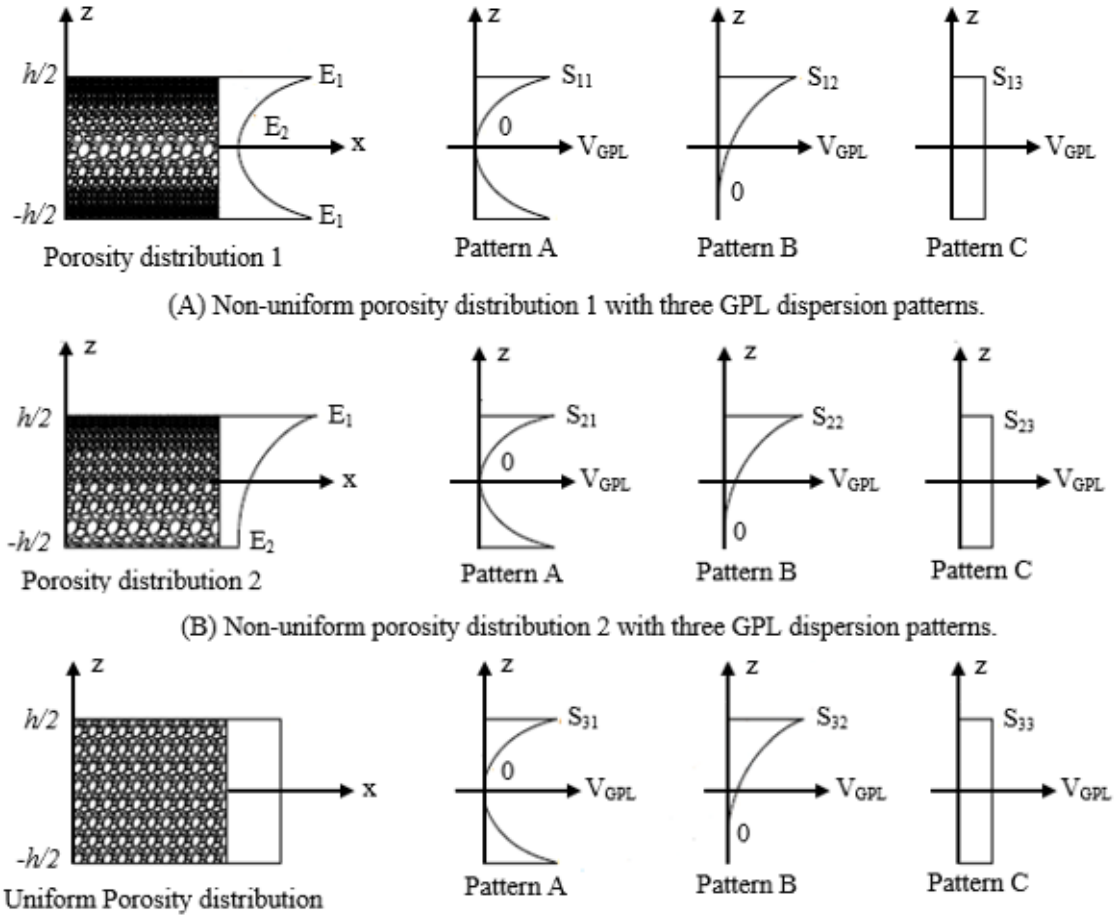

Fig. 2 Porosity distribution and GPL dispersion patterns

Also, λ(z) for uniform porosity distribution can be expressed by

$$\lambda = \frac{1}{e_0} - \frac{1}{e_0}\left(\frac{\tilde{M}/h + 0.121}{1.121}\right)^{2.3} \tag{10}$$

In which

$$\tilde{M} = \int_{-h/2}^{h/2} (1-\tilde{p})dz \tag{11}$$

According to the distribution patterns depicted in Fig. 2, the volume fraction of GPLs can be written as (i=1,2,3)

$$V_{GPL} = \begin{cases} S_{i1}\left[1-\cos(\pi z/h\right], \text{Pattern A} \\ S_{i2}\left[1-\cos(\pi z/2h + \pi/4\right], \text{Pattern B} \\ S_{i3}, \text{Pattern C} \end{cases} \tag{12}$$

The relation between the volume fraction of GPLs and their weight fraction W_{GPL} can be expressed by

$$\frac{W_{GPL}}{W_{GPL} + \frac{\rho_{GPL}}{\rho_M} - \frac{\rho_{GPL}}{\rho_M} W_{GPL}} \int_{-h/2}^{h/2} (1 - e_m \lambda(z))dz = \int_{-h/2}^{h/2} V_{GPL}(1 - e_m \lambda(z))dz \tag{13}$$

In which ρ_{GPL} and ρ_M are mass density of GPL and metal matrix, respectively. Based on Halpin-Tsai micromechanical model, it is possible to obtain material properties of GPL-reinforced metal matrix structures

$$E_1 = \frac{3}{8}\left(\frac{1+\xi_L^{GPL}\eta_L^{GPL}V_{GPL}}{1-\eta_L^{GPL}V_{GPL}}\right)E_M + \frac{5}{8}\left(\frac{1+\xi_W^{GPL}\eta_W^{GPL}V_{GPL}}{1-\eta_W^{GPL}V_{GPL}}\right)E_M \tag{14}$$

in which E_m is Young's modulus of the metal and

$$\xi_L^{GPL} = 2l_{GPL}/t_{GPL},\ \eta_L^{GPL} = \frac{(E_{GPL}/E_M)-1}{(E_{GPL}/E_M)+\xi_L^{GPL}},$$
$$\xi_W^{GPL} = 2w_{GPL}/t_{GPL},\ \eta_W^{GPL} = \frac{(E_{GPL}/E_M)-1}{(E_{GPL}/E_M)+\xi_W^{GPL}} \tag{15}$$

w_{GPL}, l_{GPL} and t_{GPL} denote GPLs' average width, length, and thickness, respectively. Finally, Poisson's ratio of GPL-reinforced metal matrix implementing rule of mixture can be expressed by

$$\upsilon_1 = \upsilon_{GPL}V_{GPL} + \upsilon_M V_M \tag{16}$$

where V_M is the volume fraction of metal matrix (V_M= 1−V_{GPL}).

3. Governing equations

In the absence of body forces, the governing equations are as follows

$$\begin{aligned}
&\frac{\partial \sigma_r}{\partial r}+\frac{1}{r}\frac{\partial \tau_{r\theta}}{\partial \theta}+\frac{\partial \tau_{rz}}{\partial z}+\frac{\sigma_r-\sigma_\theta}{r}=\rho\frac{\partial^2 u_r}{\partial t^2}\\
&\frac{\partial \tau_{r\theta}}{\partial r}+\frac{1}{r}\frac{\partial \sigma_\theta}{\partial \theta}+\frac{\partial \tau_{\theta z}}{\partial z}+\frac{2\tau_{r\theta}}{r}=\rho\frac{\partial^2 u_\theta}{\partial t^2}\\
&\frac{\partial \tau_{rz}}{\partial r}+\frac{1}{r}\frac{\partial \tau_{\theta z}}{\partial \theta}+\frac{\partial \sigma_z}{\partial z}+\frac{\tau_{rz}}{r}=\rho\frac{\partial^2 u_z}{\partial t^2}
\end{aligned} \tag{17}$$

Where $\sigma_r,\sigma_\theta,\sigma_z$ are axial stress components, $\tau_{r\theta},\tau_{\theta z},\tau_{rz}$ are shear stress components, u_r,u_θ,u_z are displacement components, ρ denotes material density and t is time. The relations between the strain and the displacement are

$$\begin{aligned}
&\varepsilon_r=\frac{\partial u_r}{\partial r},\varepsilon_\theta=\frac{u_r}{r}+\frac{1}{r}\frac{\partial u_\theta}{\partial \theta},\varepsilon_z=\frac{\partial u_z}{\partial z},\\
&\gamma_{\theta z}=\frac{\partial u_\theta}{\partial z}+\frac{1}{r}\frac{\partial u_z}{\partial \theta},\gamma_{rz}=\frac{\partial u_r}{\partial z}+\frac{\partial u_z}{\partial r},\\
&\gamma_{r\theta}=\frac{1}{r}\frac{\partial u_r}{\partial \theta}+\frac{\partial u_\theta}{\partial r}-\frac{u_\theta}{r}
\end{aligned} \tag{18}$$

Where $\varepsilon_r,\varepsilon_\theta,\varepsilon_z,\gamma_{\theta z},\gamma_{r\theta},\gamma_{rz}$ are strain components. The constitutive equations for material are (Reddy 2013):

$$\begin{Bmatrix}\sigma_r\\ \sigma_\theta\\ \sigma_z\\ \tau_{z\theta}\\ \tau_{rz}\\ \tau_{r\theta}\end{Bmatrix}=\begin{bmatrix}c_{11}&c_{12}&c_{13}&0&0&0\\ c_{12}&c_{22}&c_{23}&0&0&0\\ c_{13}&c_{23}&c_{33}&0&0&0\\ 0&0&0&c_{44}&0&0\\ 0&0&0&0&c_{55}&0\\ 0&0&0&0&0&c_{66}\end{bmatrix}\begin{Bmatrix}\varepsilon_r\\ \varepsilon_\theta\\ \varepsilon_z\\ \gamma_{z\theta}\\ \gamma_{rz}\\ \gamma_{r\theta}\end{Bmatrix} \tag{19}$$

where c_{ij} are material elastic stiffness coefficients.

Using the three-dimensional constitutive relations and the strain-displacement relations, the equations of motion in terms of displacement components for a linear elastic FG plate with infinitesimal deformations can be written as

$$\begin{aligned}
&c_{11}\frac{\partial^2 u_r}{\partial r^2}+c_{12}\left(-\frac{1}{r^2}\frac{\partial u_\theta}{\partial \theta}+\frac{1}{r}\frac{\partial^2 u_\theta}{\partial r\partial \theta}+\frac{1}{r}\frac{\partial u_r}{\partial r}-\frac{1}{r^2}u_r\right)\\
&+c_{13}\frac{\partial^2 u_z}{\partial r\partial z}+\frac{c_{66}}{r}\left(\frac{\partial^2 u_\theta}{\partial \theta\partial r}+\frac{1}{r}\frac{\partial^2 u_r}{\partial \theta^2}-\frac{1}{r}\frac{\partial u_\theta}{\partial \theta}\right)+c'_{55}\left(\frac{\partial u_r}{\partial z}+\frac{\partial u_z}{\partial r}\right)\\
&+c_{55}\left(\frac{\partial^2 u_r}{\partial z^2}+\frac{\partial^2 u_z}{\partial z\partial r}\right)+\frac{1}{r}\left[c_{11}\frac{\partial u_r}{\partial r}+\right.\\
&\left.c_{12}\left(\frac{1}{r}\frac{\partial u_\theta}{\partial \theta}+\frac{u_r}{r}\right)+c_{13}\frac{\partial u_z}{\partial z}-c_{12}\frac{\partial u_r}{\partial r}-c_{22}\left(\frac{1}{r}\frac{\partial u_\theta}{\partial \theta}+\frac{u_r}{r}\right)-c_{23}\frac{\partial u_z}{\partial z}\right]=\rho\frac{\partial^2 u_r}{\partial t^2}
\end{aligned} \tag{20}$$

$$\begin{aligned}
&c_{66}\left(\frac{\partial^2 u_\theta}{\partial r^2}-\frac{1}{r^2}\frac{\partial u_r}{\partial \theta}+\frac{1}{r}\frac{\partial^2 u_r}{\partial r\partial \theta}+\frac{1}{r^2}u_\theta-\frac{1}{r}\frac{\partial u_\theta}{\partial r}\right)\\
&+\frac{1}{r}\left[c_{12}\frac{\partial^2 u_r}{\partial \theta\partial r}+c_{22}\left(\frac{1}{r}\frac{\partial^2 u_\theta}{\partial \theta^2}+\frac{1}{r}\frac{\partial u_r}{\partial \theta}\right)+c_{23}\frac{\partial^2 u_z}{\partial \theta\partial z}\right]\\
&+c'_{44}\left(\frac{1}{r}\frac{\partial u_z}{\partial \theta}+\frac{\partial u_\theta}{\partial z}\right)+c_{44}\left(\frac{1}{r}\frac{\partial^2 u_z}{\partial z\partial \theta}+\frac{\partial^2 u_\theta}{\partial z^2}\right)\\
&+\frac{2c_{66}}{r}\left(\frac{\partial u_\theta}{\partial r}+\frac{1}{r}\frac{\partial u_r}{\partial \theta}-\frac{u_\theta}{r}\right)=\rho\frac{\partial^2 u_\theta}{\partial t^2}
\end{aligned} \tag{21}$$

$$\begin{aligned}
&c_{55}\left(\frac{\partial^2 u_r}{\partial r\partial z}+\frac{\partial^2 u_z}{\partial r^2}\right)+\frac{c_{44}}{r}\left(\frac{1}{r}\frac{\partial^2 u_z}{\partial \theta^2}+\frac{\partial^2 u_\theta}{\partial \theta\partial z}\right)\\
&+c'_{13}\frac{\partial u_r}{\partial r}+c_{13}\frac{\partial^2 u_r}{\partial z\partial r}+c'_{23}\left(\frac{1}{r}\frac{\partial u_\theta}{\partial \theta}+\frac{u_r}{r}\right)\\
&+c_{23}\left(\frac{1}{r}\frac{\partial^2 u_\theta}{\partial z\partial \theta}+\frac{1}{r}\frac{\partial u_r}{\partial z}\right)+c'_{33}\frac{\partial u_z}{\partial z}+c_{33}\frac{\partial^2 u_z}{\partial z^2}\\
&+\frac{c_{55}}{r}\left(\frac{\partial u_r}{\partial z}+\frac{\partial u_z}{\partial r}\right)=\rho\frac{\partial^2 u_z}{\partial t^2}
\end{aligned} \tag{22}$$

where $c'_{ij}=\frac{dc_{ij}}{dz}$

Eqs. (20) and (21) represent the in-plane equations of motion along the r and θ-axes, respectively; and Eq. (22) is the transverse or out-of-plane equation of motion.

The related boundary conditions are as follows:

at $z=-h/2$

$$\begin{aligned}
&\tau_{zr}=0,\tau_{z\theta}=0\\
&\sigma_z=K_w u_z-K_g\left(\frac{\partial^2 u_z}{\partial r^2}+\frac{1}{r}\frac{\partial u_z}{\partial r}+\frac{1}{r^2}\frac{\partial^2 u_z}{\partial \theta^2}\right)
\end{aligned} \tag{23}$$

at $z=h/2$

$$\tau_{zr}=0,\tau_{z\theta}=0,\sigma_z=0 \tag{24}$$

K_w and K_g are the Winkler and shearing layer elastic coefficients of the foundation. In this paper three different kinds of boundary conditions are considered for circular edges including clamped-clamped (c-c), simply supported-clamped (s-c) and free-clamped (f-c).The boundary conditions at edges are

Clamped($r=R_0$)-Clamped($r=R_1$)

$$\begin{aligned}
&\text{at}\quad r=R_1 \qquad \boldsymbol{u}_r=\boldsymbol{u}_\theta=\boldsymbol{u}_z=\boldsymbol{0}\\
&\text{at}\quad r=R_0 \qquad \boldsymbol{u}_r=\boldsymbol{u}_\theta=\boldsymbol{u}_z=\boldsymbol{0}
\end{aligned} \tag{25}$$

Simply supported($r=R_0$)-Clamped($r=R_1$):

$$\begin{aligned} &\text{at} \quad r = R_0 \qquad u_\theta = u_z = \sigma_r = 0 \\ &\text{at} \quad r = R_1 \qquad u_r = u_\theta = u_z = 0 \end{aligned} \tag{26}$$

Free(r=R_0)-Clamped(r=a):

$$\begin{aligned} &\text{at} \quad r = R_1 \qquad u_r = u_\theta = u_z = 0 \\ &\text{at} \quad r = R_0 \qquad \sigma_r = \tau_{r\theta} = \tau_{rz} = 0 \end{aligned} \tag{27}$$

4. Solution procedure

Using the geometrical periodicity of the plate, the displacement components for the free vibration analysis can be represented as

$$\begin{aligned} U_r(r,\theta,z,t) &= U_{rm}(r,z)\sin(m\pi\theta/\phi)e^{i\omega t}, \\ U_\theta(r,\theta,z,t) &= U_{\theta m}(r,z)\cos(m\pi\theta/\phi)e^{i\omega t}, \\ U_z(r,\theta,z,t) &= U_{zm}(r,z)\sin(m\pi\theta/\phi)e^{i\omega t} \end{aligned} \tag{28}$$

Where m (=0,1,…, ∞) is the circumferential wavenumber; ω is the natural frequency and i $(=\sqrt{-1})$ is the imaginary number. It is obvious that m=0 means axisymmetric vibration. At this stage the GDQ [A brief review of GDQ method is given in Appendix] rules are employed to discretize the free vibration equations and the related boundary conditions. Substituting for the displacement components from (28) and then using the GDQ rules for the spatial derivatives, the discretized form of the equations of motion at each domain grid point (r_j, z_k) with (j = 2,3,…, N_r-1) and(k =2,3,…, N_z-1) can be obtained as

Eq. (20)

$$\begin{aligned} &(c_{11})_k \sum_{n=1}^{N_r} B_{jn}^r u_{rmnk} + (c_{12})_k \left(\frac{m\pi}{r_j^2\phi} u_{\theta mjk} - \frac{m\pi}{r_j\phi} \sum_{n=1}^{N_r} A_{jn}^r u_{\theta mnk} + \frac{1}{r_j}\sum_{n=1}^{N_r} A_{jn}^r u_{rmnk} - \frac{1}{r_j^2} u_{rmjk}\right) \\ &+(c_{13})_k \sum_{n=1}^{N_r}\sum_{r=1}^{N_z} A_{jn}^r A_{kr}^z u_{zmnr} + \frac{(c_{66})_k}{r_j}\left(-\frac{m\pi}{\phi}\sum_{n=1}^{N_r} A_{jn}^r u_{\theta mnk} - \frac{m^2\pi^2}{r_j\phi^2} u_{rmjk} + \frac{m\pi}{r_j\phi} u_{\theta mjk}\right) + (c'_{55})_k \\ &\left(\sum_{n=1}^{N_z} A_{kn}^z u_{rmjn} + \sum_{n=1}^{N_r} A_{jn}^r u_{zmnk}\right) \\ &+(c_{55})_k \left(\sum_{n=1}^{N_z} B_{kn}^z u_{rmjn} + \sum_{n=1}^{N_r}\sum_{r=1}^{N_z} A_{jn}^r A_{kr}^z u_{zmnr}\right) \\ &+\frac{1}{r_j}((c_{11})_k \sum_{n=1}^{N_r} A_{jn}^r u_{rmnk} + (c_{12})_k \left(\frac{m\pi}{r_j\phi} u_{\theta mjk} + \frac{1}{r_j} u_{rmjk}\right) \\ &+(c_{13})_k \sum_{n=1}^{N_z} A_{kn} u_{zmjn} - (c_{12})_k \sum_{n=1}^{N_r} A_{jn}^r u_{rmnk} \\ &-(c_{22})_k \left(-\frac{m\pi}{r_j\phi} u_{\theta mjk} + \frac{1}{r_j} u_{rmjk}\right) - (c_{23})_k \sum_{n=1}^{N_z} A_{kn}^z u_{zmjn}) \\ &= -\rho_k \omega^2 u_{rmjk} \end{aligned} \tag{29}$$

Eq. (21)

$$\begin{aligned} &(c_{66})_k \left(\sum_{n=1}^{N_r} B_{jn}^r u_{\theta mnk} - \frac{m\pi}{r_j^2\phi} u_{rmjk} + \frac{m\pi}{r_j\phi}\sum_{n=1}^{N_r} A_{jn}^r u_{rmnk} + \frac{1}{r_j^2} u_{\theta mjk} - \frac{1}{r_j}\sum_{n=1}^{N_r} A_{jn}^r u_{\theta mnk}\right) + \frac{1}{r_j}\left((c_{12})_k \left(\frac{m\pi}{\phi}\right)\sum_{n=1}^{N_r} A_{jn}^r u_{rmnk}\right. \\ &\left.+(c_{22})_k \left(-\frac{m^2\pi^2}{r_j\phi^2} u_{\theta mjk} + \frac{m\pi}{r_j\phi} u_{rmjk}\right) + (c_{23})_k \left(\frac{m\pi}{\phi}\right)\sum_{n=1}^{N_z} A_{kn}^z u_{zmjn}\right. \\ &\left.+(c'_{44})_k \left(\frac{m\pi}{r_j\phi} u_{zmjk} + \sum_{n=1}^{N_z} A_{kn}^z u_{\theta mjn}\right)\right) \\ &+(c_{44})_k \left(\frac{m\pi}{r_j\phi}\sum_{n=1}^{N_z} A_{kn}^z u_{zmjn} + \sum_{n=1}^{N_z} B_{kn}^z u_{\theta mjn}\right) + \frac{2(c_{66})_k}{r_j} \\ &\left(\sum_{n=1}^{N_r} A_{jn}^r u_{\theta mnk} + \frac{m\pi}{r_j\phi} u_{rmjk} - \frac{u_{\theta mjk}}{r_j}\right) \\ &= -\rho_k \omega^2 u_{\theta mjk} \end{aligned} \tag{30}$$

Eq. (22)

$$\begin{aligned} &(c_{55})_k \left(\sum_{n=1}^{N_r}\sum_{r=1}^{N_z} A_{kr}^z A_{jn}^r u_{rmnr} + \sum_{n=1}^{N_r} B_{jn}^r u_{zmnk}\right) \\ &+\frac{(c_{44})_k}{r_j}\left(\frac{-m^2\pi^2}{r_j\phi^2} u_{zmjk} - \frac{m\pi}{\phi}\sum_{n=1}^{N_z} A_{kn}^z u_{\theta mjn}\right) \\ &+(c'_{13})_k \sum_{n=1}^{N_z} A_{kn}^z u_{rmjn} + (c_{13})_k \sum_{n=1}^{N_r}\sum_{r=1}^{N_z} A_{kr}^z A_{jn}^r u_{rmnr} \\ &+(c'_{23})_k \left(-\frac{m\pi}{r_j\phi} u_{\theta mjk} + \frac{u_{rmjk}}{r_j}\right) + (c_{23})_k \\ &\left(-\frac{m\pi}{r_j\phi}\sum_{n=1}^{N_z} A_{kn}^z u_{\theta mjn} + \frac{1}{r_j}\sum_{n=1}^{N_z} A_{kn}^z u_{rmjn}\right) + (c'_{33})_k \sum_{n=1}^{N_z} A_{kn}^z u_{zmjn} \\ &+(c_{33})_k \sum_{n=1}^{N_z} B_{kn}^z u_{zmjn} + \frac{(c_{55})_k}{r_j}\left(\sum_{n=1}^{N_z} A_{kn}^z u_{rmjn} + \sum_{r=1}^{N_r} A_{jr}^r u_{zmrk}\right) = -\rho_k \omega^2 u_{zmjk} \end{aligned} \tag{31}$$

Where A_{ij}^{r} , A_{ij}^{z} and B_{ij}^{r} , B_{ij}^{z} are the first and second order GDQ weighting coefficients in the r- and z- directions, respectively.

In a similar manner the boundary conditions can be discretized. For this purpose, using Eq. (28) and the GDQ discretization rules for spatial derivatives, the boundary conditions at z =-h/2 and h/2 become,

Eq. (23)

at z = -*h*/2

$$\sum_{n=1}^{N_z} A_{kn}^{z} u_{rmjn} + \sum_{n=1}^{N_r} A_{jn}^{r} u_{zmnk} = 0,$$

$$\frac{m\pi}{r_j \phi} u_{zmjk} + \sum_{n=1}^{N_z} A_{kn}^{z} u_{\theta mjn} = 0,$$

$$(c_{13})_k \left(\sum_{n=1}^{N_r} A_{jn}^{r} u_{rmnk}\right) + (c_{23})_k \left(-\frac{m\pi}{r_j \phi} u_{\theta mjk} + \frac{1}{r_j} u_{rmjk}\right) \quad (32)$$

$$+(c_{33})_k \left(\sum_{n=1}^{N_z} A_{kn}^{z} u_{zmjn}\right) - K_w u_{zmjk} + K_g$$

$$\left(\sum_{n=1}^{N_r} B_{jn}^{r} u_{zmnk} + \frac{1}{r_j} \sum_{n=1}^{N_r} A_{jn}^{r} u_{zmnk} - \frac{m^2\pi^2}{r_j^2 \phi^2} u_{zmjk}\right) = 0$$

Eq. (24):

at *z* = *h*/2

$$\sum_{n=1}^{N_z} A_{kn}^{z} u_{rmjn} + \sum_{n=1}^{N_r} A_{jn}^{r} u_{zmnk} = 0,$$

$$\frac{m\pi}{r_j \phi} u_{zmjk} + \sum_{n=1}^{N_z} A_{kn}^{z} u_{\theta mjn} = 0,$$

$$(c_{13})_k \left(\sum_{n=1}^{N_r} A_{jn}^{r} u_{rmnk}\right) + (c_{23})_k \left(-\frac{m\pi}{r_j \phi} u_{\theta mjk} + \frac{1}{r_j} u_{rmjk}\right) \quad (33)$$

$$+(c_{33})_k \left(\sum_{n=1}^{N_z} A_{kn}^{z} u_{zmjn}\right) = 0$$

where k = 1 at z = -*h*/2 and k = N_z at z = *h*/2, andj = 1,2, . . ., N_r. The boundary conditions at r = R_0 and R_1 stated in (25-27) become,

Simply supported (S)

$$u_{zmjk} = 0, u_{\theta mjk} = 0,$$

$$(c_{11})_k \left(\sum_{n=1}^{N_r} A_{jn}^{r} u_{rmnk}\right) + (c_{12})_k \left(-\frac{m\pi}{r_j \phi} u_{\theta mjk} + \frac{1}{r_j} u_{rmjk}\right) \quad (34.1)$$

$$+(c_{13})_k \left(\sum_{n=1}^{N_z} A_{kn}^{z} u_{zmjn}\right) = 0$$

Clamped (C)

$$u_{rmjk} = 0, u_{\theta mjk} = 0, u_{zmjk} = 0 \quad (34.2)$$

Free (F)

$$(c_{11})_k \sum_{n=1}^{N_r} A_{jn}^{r} u_{rmnk} + (c_{12})_k \left(-\frac{m\pi}{r_j \phi} u_{\theta mjk} + \frac{1}{r_j} u_{rmjk}\right)$$

$$+(c_{13})_k \sum_{n=1}^{N_z} A_{kn}^{z} u_{zmjn} = 0,$$

$$\sum_{n=1}^{N_r} A_{jn}^{r} u_{\theta mnk} + \frac{m\pi}{\phi} u_{rmjk} - u_{\theta mjk} = 0, \quad (34.3)$$

$$\sum_{n=1}^{N_z} A_{kn}^{z} u_{rmjn} + \sum_{n=1}^{N_r} A_{jn}^{r} u_{zmnk} = 0$$

In the above equations k = 2, . . ., N_z-1; also j = 1 at r = R_0 and j = N_r at r = R_1.

In order to carry out the eigenvalue analysis, the domain and boundary degrees of freedom are separated and in vector forms they are denoted as {d} and {b}, respectively. Based on this definition, the discretized form of the equilibrium equations and the related boundary conditions take the following forms,

Equations of motion (29-31)

$$\left[\left[K_{db}\right]\left[K_{dd}\right]\right]\begin{Bmatrix}\{b\}\\ \{d\}\end{Bmatrix} - \omega^2 [M]\{d\} = \{0\} \quad (35)$$

Boundary conditions (21, 22) and (23.1-3)

$$\left[K_{bd}\right]\{d\} + \left[K_{bb}\right]\{b\} = \{0\} \quad (36)$$

Eliminating the boundary degrees of freedom in Eq. (35) using Eq. (36), this equation become

$$\left(\left[K\right] - \omega^2 \left[M\right]\{d\}\right) = \{0\} \quad (37)$$

where $[K] = [K_{dd}] - [K_{db}][K_{bb}]^{-1}[K_{bd}]$ The above eigenvalue system of equations can be solved to find the natural frequencies and mode shapes of the plates.

5. Convergence and comparison studies

In this section, the convergence behavior and accuracy of the method in evaluating the non-dimensional natural frequencies of isotropic and FGM annular sector plates with different set of boundary conditions along the circular edges are investigated.

Leissa *et al*. (1993, 1995) provided the exact results for sector plates with a re-entrant corner, based on the Mindlin plate theory. As a first example, the comparative studies of the fundamental frequency parameters are given in Table 1. It is seen from Table 1 that for thin plates $(h/R_1 = 0.01)$

Table 1 Comparison of fundamental frequency parameter $(\Omega = \omega R_1^2\sqrt{\rho h/D})$ for flexural vibration of annular sector plates with two straight edges simply supported for $R_0/R_1 = 0.5$

$\phi(\deg)$	h/R_1	Theories	C-C	F-C	F-S
195	0.01	Leissa *et al*. (1995)	90.0837	21.4263	10.8761
		Zhou *et al*. (2009)	90.1125	21.4074	10.8522
		Present	90.1123	21.4076	10.8524
	0.2	Leissa *et al*. 1995	70.8090	19.9986	10.2268
		Zhou *et al.* (2009)	71.9146	20.0967	10.2386
		Present	71.9143	20.0968	10.2384
	0.4	Leissa *et al*. (1995)	48.6618	17.5822	9.3661
		Zhou *et al.* (2009)	50.0059	17.7636	9.3961
		Present	50.0056	17.7638	9.3962
210	0.01	Leissa *et al*. (1995)	89.9678	20.9496	10.2631
		Zhou *et al*. (2009)	90.0265	20.9368	10.2418
		Present	90.0264	20.9369	10.2416
	0.2	Leissa *et al.* (1995)	70.7344	19.6097	9.6643
		Zhou *et al*. (2009)	71.8406	19.7064	9.6751
		Present	71.8406	19.7063	9.6752
	0.4	Leissa *et al.* (1995)	48.6117	17.2943	8.8769
		Zhou *et al.* (2009)	49.9566	17.4733	8.9043
		Present	49.9564	17.4735	8.9041
270	0.01	Leissa *et al*. (1995)	89.6828	19.7282	8.5788
		Zhou *et al.* (2009)	89.7655	19.7258	8.5635
		Present	89.7653	19.7259	8.5633
	0.2	Leissa *et al.* (1995)	70.5516	18.6218	8.1304
		Zhou *et al*. (2009)	71.6588	18.7149	8.1386
		Present	71.6586	18.7150	8.1387
	0.4	Leissa *et al*. 1995	48.4901	16.5657	7.5461
		Zhou *et al*. (2009)	49.8361	16.7386	7.5670
		Present	49.8360	16.7387	7.5670
360	0.01	Leissa *et al.* (1995)	89.4931	18.8711	7.2502
		Zhou *et al.* (2009)	89.6519	18.8831	7.2418
		Present	89.6520	18.8829	7.2421
	0.2	Leissa *et al.* (1995)	70.4307	17.9366	6.9363
		Zhou *et al.* (2009)	71.5435	18.0283	6.9426
		Present	71.5433	18.0285	6.9423
	0.4	Leissa *et al.* (1995)	48.4105	16.0630	6.5171
		Zhou *et al.* (2009)	49.7559	16.2316	6.5332
		Present	49.7561	16.2315	6.5331

there is an excellent agreement between the present 3-D solutions and the classical solutions. For moderately thick plates $(h/R_1 = 0.2)$ the present 3-D solutions also agree quite well with the Mindlin solutions. For very thick plates $(h/R_1 = 0.4)$ the discrepancies increase, particularly for c-c plates. It is found that only nineteen DQ grid points in each direction (r and z) can yield accurate results. The same problem has been analyzed by D. Zhou *et al.* (2009). It is obvious that the error of the Mindlin plate theory increases with the increase of the plate thickness, especially for very thick plates $(h/R_1 \geq 0.4)$. The two-dimensional theories, such as the classical plate theory, the first and the higher order shear deformation plate theories neglect transverse normal deformations, and generally assume that a plane stress state of deformation prevails in the plate. These assumptions may be appropriate for thin plates but do not give good results for thick plates. It is seen from Table 1 that the maximum differences between the 3-D solutions and the Mindlin solutions occur at the clamped-clamped plates. A numerical value of $N_r = N_z = 19$ is used for the next studies. As the second example, the convergence behavior and accuracy of the method for lowest non-dimensional frequency parameter $(\varpi = \omega h\sqrt{\rho/C_{11}})$ of thick FG annular sector plates with two different set of circular edges conditions including clamped-clamped and clamped - simply supported are studied in Tables 2 and 3. The results are compared with those of the three-dimensional elasticity solutions of Nie and Zhong (2008) which were obtained using the State space method (S.S.M). It is assumed that the material properties vary exponentially $(c_{ij}(z) = c_{ij}^M e^{(\frac{\lambda z}{h})}, \rho(z) = \rho^M e^{(\frac{\lambda z}{h})})$ through the thickness of the plate. Superscripts *M* denote the material properties of the bottom surface of the plate, λ is the material property graded index. One can see that an excellent agreement exists between the converged results of the presented approach and the other one. The material property and geometry parameters of GPLs are W_{GPL}=1.5 μm, l_{GPL}=2.5

Table 2 The lowest non-dimensional frequency parameter $\left(\varpi = \omega h\sqrt{\rho/C_{11}}\right)$ for FGMs annular sector plates having clamped ($r=R_0$) and clamped ($r=R_1$) conditions

ϕ(deg)	h/R_1	R_0/R_1	m		λ				
					1	2	3	4	5
195	0.1	0.1	1	Nie and Zhong (2008)	0.0663	0.0622	0.0566	0.0505	0.0446
				Present	0.0664	0.0623	0.0564	0.0505	0.0445
			2	Nie and Zhong (2008)	0.0795	0.0746	0.0677	0.0603	0.0531
				Present	0.0793	0.0747	0.0679	0.0603	0.0530
		0.3	1	Nie and Zhong (2008)	0.1041	0.0980	0.0895	0.0801	0.0710
				Present	0.1039	0.0979	0.0897	0.0800	0.0710
			2	Nie and Zhong (2008)	0.1104	0.1039	0.0948	0.0849	0.0753
				Present	0.1105	0.1039	0.0950	0.0850	0.0752
	0.3	0.1	1	Nie and Zhong (2008)	0.4040	0.3862	0.3611	0.3329	0.3046
				Present	0.4041	0.3863	0.3610	0.3327	0.3048
			2	Nie and Zhong (2008)	0.5013	0.4781	0.4455	0.4091	0.3730
				Present	0.5011	0.4779	0.4455	0.4092	0.3729
		0.3	1	Nie and Zhong (2008)	0.5645	0.5436	0.5137	0.4796	0.4450
				Present	0.5646	0.5435	0.5138	0.4796	0.4452
			2	Nie and Zhong (2008)	0.6077	0.5840	0.5504	0.5125	0.4744
				Present	0.6079	0.5842	0.5505	0.5124	0.4746
210	0.1	0.1	1	Nie and Zhong (2008)	0.0659	0.0619	0.0563	0.0502	0.0443
				Present	0.0660	0.0621	0.0561	0.0501	0.0444
			2	Nie and Zhong (2008)	0.0766	0.0719	0.0653	0.0581	0.0512
				Present	0.0765	0.0721	0.0654	0.0583	0.0510
		0.3	1	Nie and Zhong (2008)	0.1039	0.0978	0.0892	0.0799	0.0708
				Present	0.1037	0.0977	0.0895	0.0800	0.0706
			2	Nie and Zhong (2008)	0.1090	0.1027	0.0937	0.0839	0.0744
				Present	0.1092	0.1029	0.0935	0.0839	0.0745
	0.3	0.1	1	Nie and Zhong (2008)	0.4002	0.3827	0.3580	0.3302	0.3023
				Present	0.4000	0.3829	0.3582	0.3304	0.3023
			2	Nie and Zhong (2008)	0.4832	0.4608	0.4294	0.3943	0.3594
				Present	0.4833	0.4606	0.4296	0.3944	0.3595
		0.3	1	Nie and Zhong (2008)	0.5630	0.5421	0.5123	0.4784	0.4439
				Present	0.5633	0.5421	0.5121	0.4784	0.4440
			2	Nie and Zhong (2008)	0.5990	0.5756	0.5428	0.5056	0.4682
				Present	0.5991	0.5755	0.5429	0.5057	0.4683

μm, t_{GPL} l.5 nm, E_{GPL}=1.01 TPa, ρ_{GPL}=1062.5 kg/m3, $\boldsymbol{\upsilon}$=0.186 (Rafiee *et al.* 2009, Liu *et al.* 2007), and the material properties of metal are E_M = 130 GPa, ρ_M = 8960 kg/m3, $\boldsymbol{\upsilon}_M$= 0.34 (Kitipornchai *et al*. 2017).

In this study, the non-dimensional natural frequency is as follows

$$\Omega = \omega R_1^2\sqrt{\rho_m h/D_m} \ , \ D_m = E_m h^3/12(1-\upsilon_m^2) \tag{38}$$

The non-dimensional natural frequency, Winkler and shearing layer elastic coefficients are as follows

$$K_g = k_g R_1^{\ 2}/D_m \ , \ K_w = k_w R_1^{\ 4}/D_m \tag{39}$$

where ρ_M, E_M and $\boldsymbol{\upsilon}_M$ are mechanical properties of Copper.

6. Benchmark results

The influences of the sector angle on the fundamental frequency parameters of GPLs-reinforcement annular sector plates on two-parameter elastic foundation with different circular edges boundary conditions are shown in Fig. 3. It is obvious that for all types of boundary condition, with increasing the sector angle, the frequency parameters decrease. It is observed that the natural frequency of Clamped-Clamped sector plates is significantly higher than those of sector plates with Simply supported-Clamped and Free-Clamped boundary conditions. As expected, increasing the degrees of freedom in the edges, decreases the natural frequencies. The variation of inner-to-outer radius ratio (R_0/R_1) with the frequency parameters of a Clamped-Clamped, Simply supported-Clamped and Free-Clamped GPLs-reinforcement annular sector plates for different values of h/R_1 ratios is shown in Figs. 4-6. According to these figures, the general behavior of the frequency parameters of the plates for all R_0/R_1 ratios is that the effects of the h/R_1 ratios are more prominent at high inner-to-outer radius ratios. As it is observed, the frequency parameter decreases rapidly with the decrease of R_0/R_1 ratio and then remains almost unaltered for the R_0/R_1<0.3. The influences of the coefficient of porosity on the fundamental frequency parameters of GPLs-reinforcement annular sector plates with different circular boundary conditions are investigated

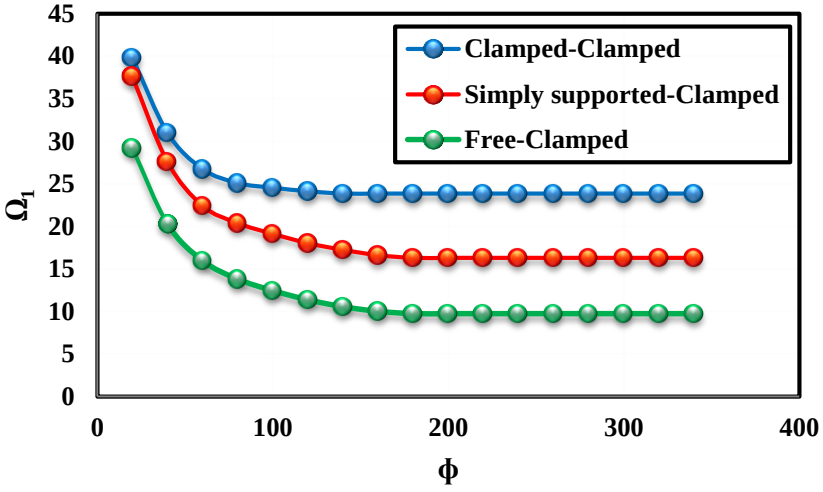

Fig. 3 Influence of the sector angle on the non-dimensional natural frequency parameter of GPLs-reinforcement sectorial plates (K_w=100, K_g=0, R_0/R_4=0.6, h/R_1=0.1, e=0.5)

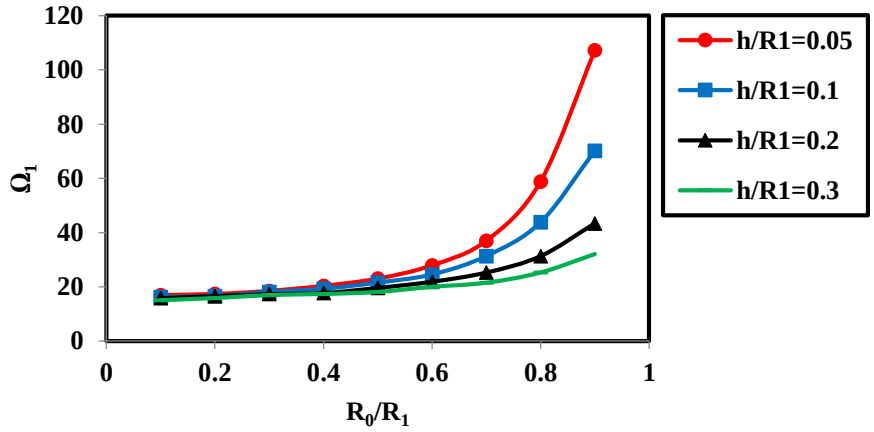

Fig. 4 Variation of natural frequency of Uniform GPL-reinforced sectorial plates versus inner-to-outer radius ratios (R_0/R_1) for C-C boundary condition at the circular edges (h/R_1=0.1, e=0.5, GPL weight fraction wt. 1%, K_w=100, K_g=0, ϕ=100º)

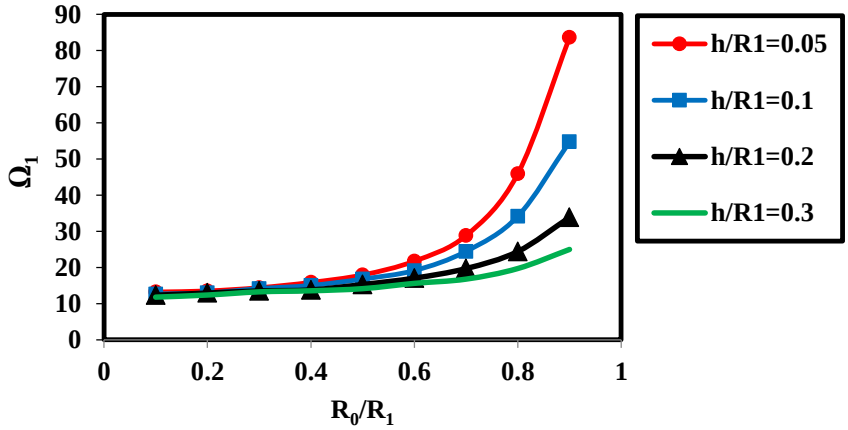

Fig. 5 Variation of natural frequency of Uniform GPL-reinforced sectorial plates versus inner-to-outer radius ratios (R_0/R_1) for S-C boundary condition at the circular edges (h/R_1=0.1, e=0.5, GPL weight fraction wt. 1%, K_w=100, K_g=0, ϕ=100º)

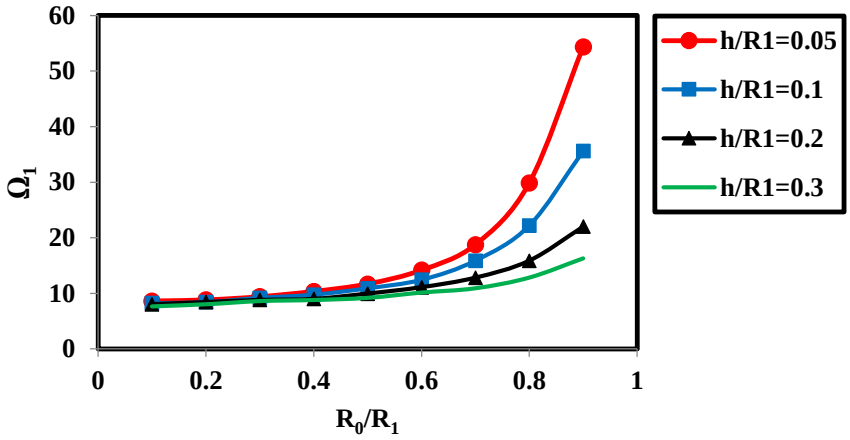

Fig. 6 Variation of natural frequency of Uniform GPL-reinforced sectorial plates versus inner-to-outer radius ratios (R_0/R_1) for F-C boundary condition at the circular edges (h/R_1=0.1, e=0.5, GPL weight fraction wt. 1%, K_w=100, K_g=0, ϕ=100°)

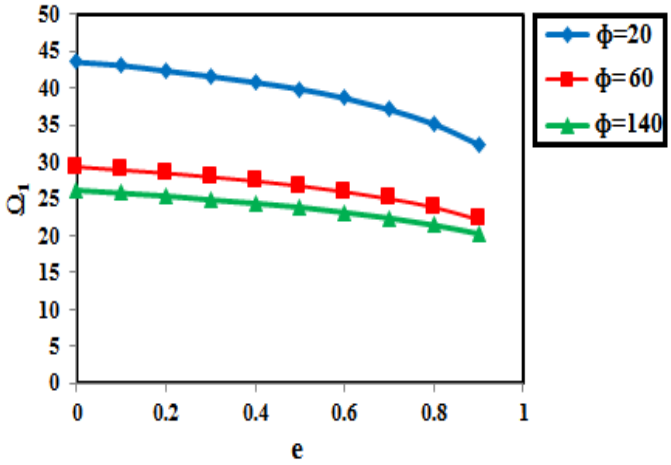

Fig. 7 The influence of plate porosity and sector angle on the natural frequency of C-C sectorial plates (h/R_1=0.1, GPL weight fraction wt. 1%, Kw=100, Kg=0)

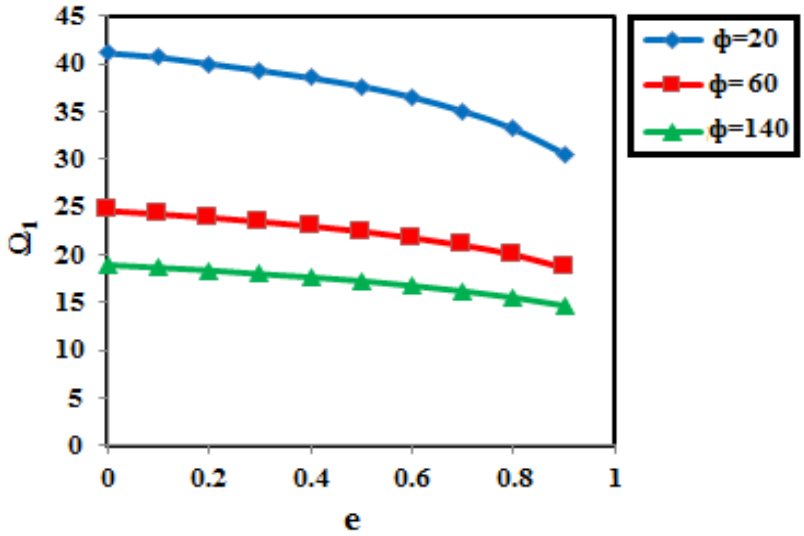

Fig. 8 The influence of plate porosity and sector angle on the natural frequency of S-C sectorial plates (h/R_1=0.1, GPL weight fraction wt. 1%, Kw=100, Kg=0)

Table 3 The lowest non-dimensional frequency parameter $\left(\varpi = \omega h\sqrt{\rho/C_{11}}\right)$ for FGMs annular sector plates having clamped ($r=R_0$) and simply supported ($r=R_1$) conditions

ϕ(deg)	h/R_1	R_0/R_1	m		λ				
					1	2	3	4	5
195	0.1	0.1	1	Nie and Zhong 2008	0.0442	0.0412	0.0372	0.0329	0.0289
				Present	0.0444	0.0411	0.0374	0.0329	0.0287
			2	Nie and Zhong 2008	0.0582	0.0542	0.0488	0.0431	0.0377
				Present	0.0584	0.0544	0.0487	0.0429	0.0378
		0.3	1	Nie and Zhong 2008	0.0727	0.0680	0.0617	0.0548	0.0484
				Present	0.0726	0.0682	0.0618	0.0548	0.0485
			2	Nie and Zhong 2008	0.0802	0.0751	0.0680	0.0604	0.0532
				Present	0.0803	0.0750	0.0680	0.0605	0.0531
	0.3	0.1	1	Nie and Zhong 2008	0.3152	0.2948	0.2687	0.2418	0.2166
				Present	0.3153	0.2949	0.2689	0.2416	0.2164
			2	Nie and Zhong 2008	0.4316	0.4039	0.3679	0.3304	0.2951
				Present	0.4314	0.4041	0.3680	0.3304	0.2950
		0.3	1	Nie and Zhong 2008	0.4565	0.4245	0.3922	0.3600	0.3290
				Present	0.4564	0.4243	0.3920	0.3600	0.3290
			2	Nie and Zhong 2008	0.5198	0.4828	0.4442	0.4059	0.3693
				Present	0.5199	0.4826	0.4442	0.4060	0.3690
210	0.1	0.1	1	Nie and Zhong 2008	0.0438	0.0409	0.0369	0.0327	0.0287
				Present	0.0437	0.0407	0.0371	0.0329	0.0287
			2	Nie and Zhong 2008	0.0552	0.0515	0.0463	0.0408	0.0357
				Present	0.0550	0.0517	0.0464	0.0408	0.0356
		0.3	1	Nie and Zhong 2008	0.0724	0.0678	0.0614	0.0546	0.0482
				Present	0.0722	0.0679	0.0615	0.0547	0.0481
			2	Nie and Zhong 2008	0.0787	0.0736	0.0667	0.0593	0.0522
				Present	0.0786	0.0735	0.0669	0.0594	0.0523
	0.3	0.1	1	Nie and Zhong 2008	0.3103	0.2904	0.2648	0.2384	0.2137
				Present	0.3101	0.2905	0.2650	0.2384	0.2135
			2	Nie and Zhong 2008	0.4105	0.3840	0.3495	0.3137	0.2800
				Present	0.4106	0.3842	0.3493	0.3138	0.2801
		0.3	1	Nie and Zhong 2008	0.4538	0.4221	0.3901	0.3582	0.3275
				Present	0.4540	0.4221	0.3900	0.3584	0.3277
			2	Nie and Zhong 2008	0.5077	0.4715	0.4340	0.3968	0.3613
				Present	0.5076	0.4716	0.4342	0.3969	0.3612

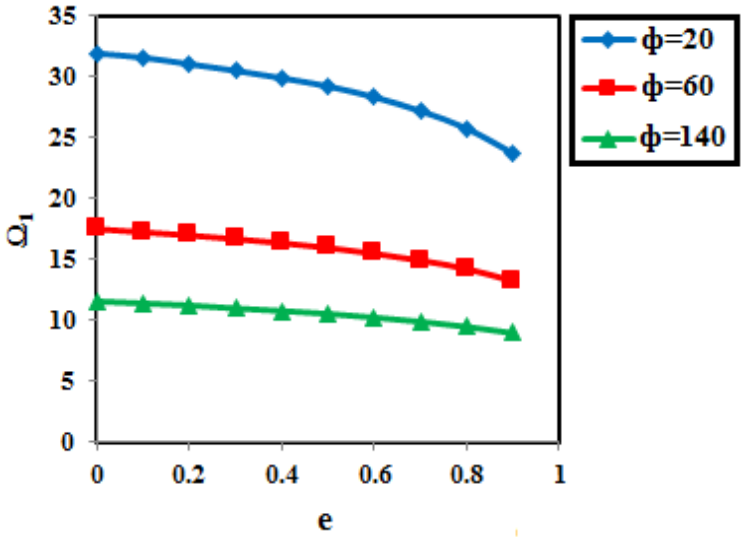

Fig. 9 The influence of plate porosity and sector angle on the natural frequency of F-C sectorial plates (h/R_1=0.1, GPL weight fraction wt. 1%, Kw=100, Kg=0)

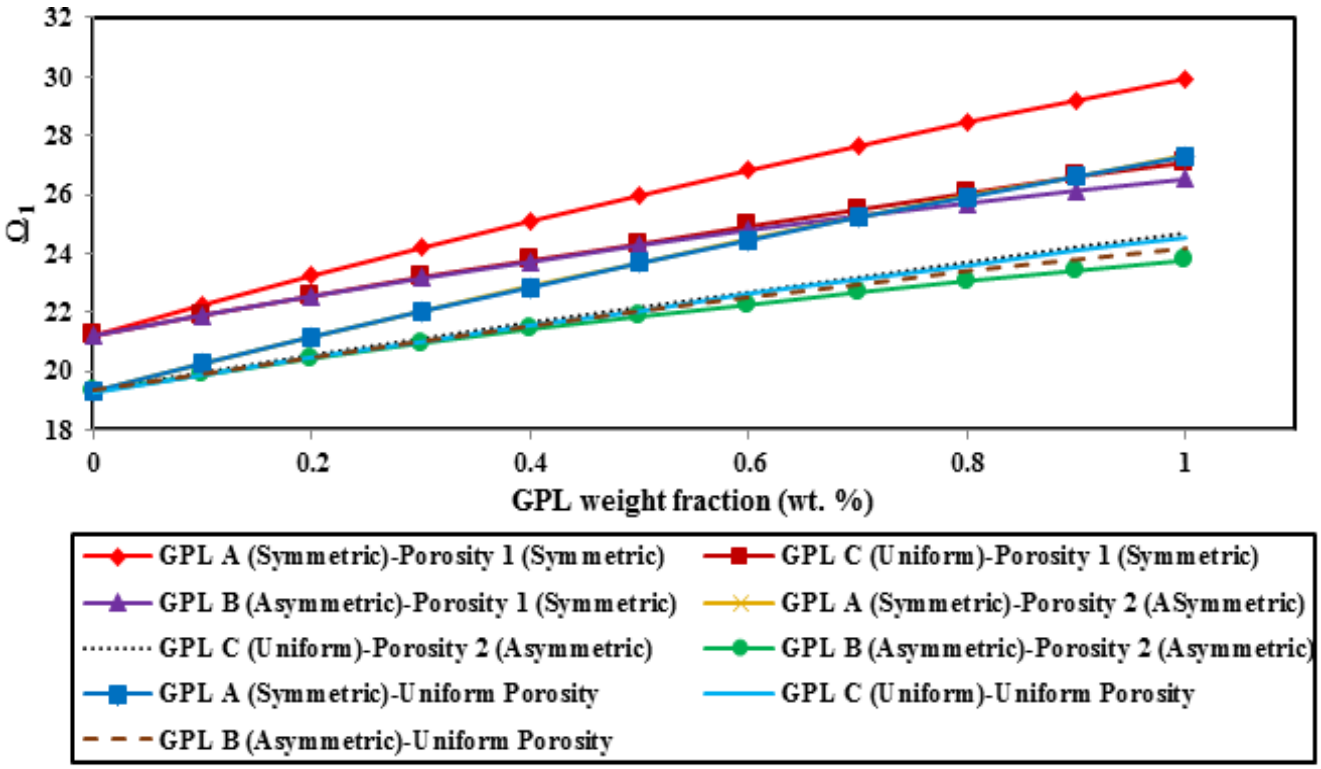

Fig. 10 The effect of GPL on the fundamental frequency of nanocomposite C-C sectorial plates (h/R_1=0.1, e=0.5, K_w=100, K_g=0, ϕ=100°)

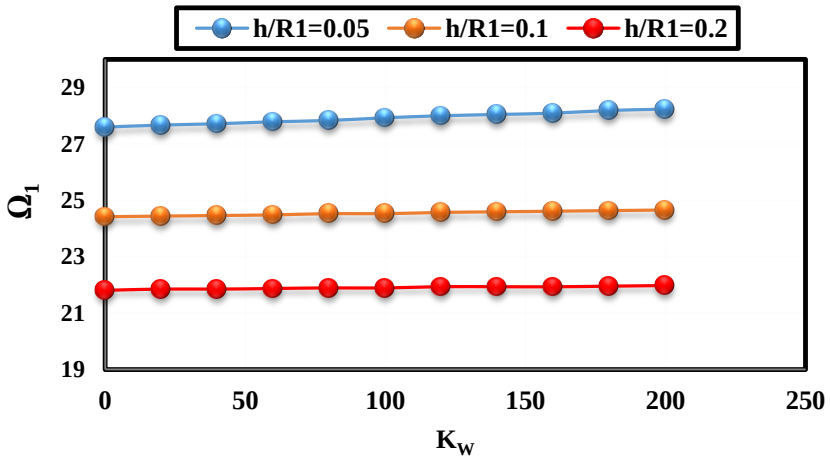

Fig. 11 Variation of dimensionless frequency of sectorial plates versus Winkler elastic parameter for various thickness-to-outer radius ratios (e=0.5, GPL weight fraction wt. 1%, K_g=0, ϕ=100°).

in Figs. 7-9. Based on the results the frequency parameter is sensitive to the value of coefficient of plate porosity significantly as well as the sector angle. The results imply that the frequency parameter decreases as the coefficient of plate porosity increases. The combined effects of porosity distribution and GPL distribution pattern on the fundamental frequency are investigated in Fig. 10 in which the fundamental natural frequency at various GPL weight fractions is presented. Symmetric GPL pattern A is proved to be the best dispersion method, followed by the uniform pattern C which is slightly better than the asymmetric pattern B. Results indicate that plate with non-uniform symmetric porosity distribution 1 and symmetric GPL pattern A have the largest fundamental frequencies, i.e., the highest effective stiffness under the same GPL weight fraction, suggesting that a nanocomposite plate in which both internal pores and nanofillers are symmetrically distributed can offer the best structural performance. It should be noted this tendency has been seen in other types of boundary conditions but for the sake of brevity, they are

not reported here. It is observed that the maximum vibration frequency obtained in the case of symmetric porosity and GPL distribution, while the minimum vibration frequency is obtained using uniform porosity distribution. Figure 11 indicates the effect of Winkler and Pasternak foundation parameters when e_0=0.5, GPL weight fraction wt. 1% and e=0.5. A Clamped-Clamped annular sector plate with uniform porosities has been considered in this figure. It is crystal clear that higher values of Winkler foundation constant leads to increase in bending rigidity and natural frequency of the annular sector plates.

6. Conclusions

This paper deals with vibration analysis of functionally graded porous nanocomposite annular sector plate resting on elastic foundation where the internal pores and graphene platelets (GPLs) are distributed in the matrix uniformly or non-uniformly according to three different patterns. The elastic foundation is considered as a Pasternak model with adding a shear layer to the Winkler model. Three complicated equations of motion for the plate under consideration are semi-analytically solved by using 2-D differential quadrature method. The annular sector plate is assumed to be simply supported in the radial edges while any arbitrary boundary conditions are applied to the other two circular edges including simply supported, clamped and free. Using the 2-D differential quadrature method in the r- and z-directions, allows one to deal with FG plates with arbitrary thickness distribution of material properties and also to implement the effects of the elastic foundations as a boundary condition on the lower surface of the plate efficiently and in an exact manner. The fast rate of convergence and accuracy of the method are investigated through the different solved examples. From this study some conclusions can be made as following:

- It is observed that the maximum vibration frequency obtained in the case of symmetric porosity and GPL distribution, while the minimum vibration frequency is obtained using uniform porosity distribution.
- It is obvious that for all types of boundary condition, with increasing the sector angle, the frequency parameters decrease.
- As expected, increasing the degrees of freedom in the edges, decreases the natural frequencies.
- As it is observed, the frequency parameter decreases rapidly with the decrease of R_0/R_1 ratio and then remains almost unaltered for the R_0/R_1<0.3.
- Based on the results the frequency parameter is sensitive to the value of coefficient of plate porosity significantly as well as the sector angle. The results imply that the frequency parameter decreases as the coefficient of plate porosity increases.
- It is observed that higher values of Winkler foundation constant leads to increase in bending rigidity and natural frequency of the annular sector plates.

Results show that for better understanding of mechanical behavior of nanocomposite plates, it is crucial to consider porosities inside the material structure.

Acknowledgments

The research described in this paper, Founded within the project No. A201901046 and supported by “the talent training project of Hebei province”.

References

Ahmed Houari, M.S., Bessaim, A., Bernard, F., Tounsi, A. and Mahmoud, S.R. (2018), “Buckling analysis of new quasi-3D FG nanobeams based on nonlocal strain gradient elasticity theory and variable length scale parameter”, *Steel Compos. Struct*., **28**(1), 13-24. https://doi.org/10.12989/scs.2018.28.1.013.

Affdl Halpin, J.C. and Kardos, J.L. (1976), “The Halpin-Tsai equations: A review”, *Polym. Eng. Sci.,***16**(5), 344-352. https://doi.org/10.1002/pen.760160512.

Arefi, M. (2015), “Elastic solution of a curved beam made of functionally graded materials with different cross sections’, *Steel Compos. Struct*., **18**(3), 659-672. https://doi.org/10.12989/scs.2015.18.3.659.

Rao, M.N., Guruswamy, P. and Sampath Kumaran, K.S. (1977), “Finite element analysis of thick annular and sector plates”, *Nucl. Eng. Des*., **41**(2), 247-255. https://doi.org/10.1016/0029-5493(77)90113-3.

Barka, M., Benrahou, K.H., Bakora, A. and Tounsi, A. (2016), “Thermal post-buckling behavior of imperfect temperature-dependent sandwich FGM plates resting on Pasternak elastic foundation”, *Steel Compos. Struct*., **22**(1), 91-112. https://doi.org/10.12989/scs.2016.22.1.091.

Bouguenina, O., Belakhdar, K., Tounsi, A. and Bedia, E.A.A. (2015), “Numerical analysis of FGM plates with variable thickness subjected to thermal buckling”, *Steel Compos. Struct*., **19**(3), 679-695. https://doi.org/10.12989/scs.2015.19.3.679.

Bennai, R., Ait Atmane, H. and Tounsi, A. (2015), “A new higher-order shear and normal deformation theory for functionally graded sandwich beams”, *Steel Compos. Struct*., **19**(3), 521-546. https://doi.org/10.12989/scs.2015.19.3.521.

Benson, P.R. and Hinton, E. (1976), “A thick finite strip solution for static, free vibration and stability problems”, *Int. J. Numer. Method. Eng*., **10**(3), 665-678. https://doi.org/10.1002/nme.1620100314.

Bert, C.W. and Malik, M. (1996), “Differential quadrature method in computational mechanics: a review”, *Appl. Mech. Rev.*, **49**, 1-27. https://doi.org/10.1115/1.3101882.

Bouchafa, A., Bouiadjra, M.B., Houari, M.S.A. and Tounsi, A. (2015), “Thermal stresses and deflections of functionally graded sandwich plates using a new refined hyperbolic shear deformation theory”, *Steel Compos. Struct*., **18**(6), 1493-1515. https://doi.org/10.12989/scs.2015.18.6.1493.

Chen, C.S., Liu, F.H. and Chen, W.R. (2017), “vibration and stability of initially stressed sandwich plates with FGM face sheets in thermal environments”, *Steel Compos. Struct*., **23**(3), 251-261. https://doi.org/10.12989/scs.2017.23.3.251.

Cheung, M.S. and Chan, M.Y.T. (1981), “Static and dynamic analysis of thin and thick sectorial plates by the finite strip method”, *Comput. Struct*., **14**(1-2), 79-88. https://doi.org/10.1016/0045-7949(81)90086-9.

Fidelus, J.D., Wiesel, E., Gojny, F.H., Schulte, K. and Wagner, H.D. (2005), "Thermo-mechanical properties of randomly oriented carbon/epoxy nanocomposites", *Compos. Part A*, **36**, 1555-1561. https://doi.org/10.1016/j.compositesa.2005.02.006.

Finot, M. and Suresh, S. (1996), "Small and large deformation of thick and thin-film multilayers: effect of layer geometry, plasticity and compositional gradients", *J. Mech. Phys. Solids*, **44**(5), 683-721. https://doi.org/10.1016/0022-5096(96)84548-0.

Ghavamian, A., Rahmandoust, M. and Öchsner, A. (2012), 62, "A numerical evaluation of the influence of defects on the elastic modulus of single and multi-walled carbon nanotubes", *Comput. Mater. Sci*., **62**, 110-116. https://doi.org/10.1016/j.commatsci.2012.05.003.

Gojny, F.H., Wichmann, M.H.G., Fiedler, B. and Schulte, K. (2005), "Influence of different carbon nanotubes on the mechanical properties of epoxy matrix composites-A comparative study", *Compos. Sci. Technol.*, **65**, 2300-2313.https://doi.org/10.1016/j.compscitech.2005.04.021.

Guruswamy, P. and Yang, T.Y. (1979), "A sector finite element for dynamic analysis of thick plates, *J. Sound Vib*., **62**(4), (1979) 505-516. https://doi.org/10.1016/0022-460X(79)90459-0.

Halpin, J.C. and Tsai, S.W. (1969), "Effects of environmental factors on composite materials", *AFML-TR*-67-423.

Houmat, A. (2001), "A sector Fourier p-element applied to free vibration analysis of sectorial plates", *J. Sound Vib*., **243**(2), 269-282. https://doi.org/10.1006/jsvi.2000.3410.

Kim, C.S. and Dickinson, S.M. (1989), "On the free, transverse vibration of annular and circular, thin, sectorial plates subjected to certain complicating effects", *J. Sound Vib.*, **134**(3), 407-421. https://doi.org/10.1016/0022-460X(89)90566-X.

Kitipornchai, S., Chen, D., Yang, J. (2017), "Free vibration and elastic buckling of functionally graded porous beams reinforced by graphene platelets", *Mater. Design*, **116**, 656-665. https://doi.org/10.1016/j.matdes.2016.12.061.

Koizumi, M. (1993), "The concept of FGM", *Ceram. Trans. Funct. Grad. Mater*., **34**, 3-10.

Leissa, A.W., McGee, O.G. and Huang, C.S. (1993), "Vibrations of sectorial plates having corner stress singularities", *J. Appl. Mech. T. ASME*, **60**(1), 134-140. https://doi.org/10.1115/1.2900735.

Liew, K.M. and Lam, K.Y. (1993), "On the use of 2-d orthogonal polynomials in the Rayleigh-Ritz method for flexural vibration of annular sector plates of arbitrary shape", *Int. J. Mech. Sci*., **35**(2), 129-139. https://doi.org/10.1016/0020-7403(93)90071-2.

Liew, K.M. and Liu, F.L. (2000), "Differential quadrature method for vibration analysis of shear deformable annular sector plates", *J. Sound Vib*., **230**(2), 335-356. https://doi.org/10.1006/jsvi.1999.2623.

Liu, R., Wang, L. (2015), "Thermal vibration of a single-walled carbon nanotube predicted by semiquantum molecular dynamics", *Phys. Chemistry Chemical Phys*., 7. https://doi.org/10.1039/C4CP05495D.

Marin, M. and Craciun E.M. (2017), "Uniqueness results for a boundary value problem in dipolar thermoelasticity to model composite materials", *Compos. Part B: Eng*., **126**, 27-37.

Marin, M., Baleanu, D. and Vlase, S. (2017), "Effect of microtemperatures for micropolar thermoelastic bodies", *Struct. Eng. Mech.*, **61**(3), 381-387. https://doi.org/10.12989/sem.2017.61.3.381.

Marin, M., Ellahi, R. and Chirila, A. (2017), "On solutions of Saint-Venant's problem for elastic dipolar bodies with voids", *Carpathian J. Math.*, **32**(2), 219-232.

Marin, M. (2010), "A domain of influence theorem for microstretch elastic materials, *Nonlinear Anal. Real World Appl.*, **11**(5), 3446-3452. https://doi.org/10.1016/j.nonrwa.2009.12.005.

Marin, M. and Lupu, M. (1998), "On harmonic vibrations in thermoelasticity of micropolar bodies", *J. Vib. Control*, **4**(5), 507-518. https://doi.org/10.1177/107754639800400501.

Marin, M. and Marinescu, C. (1998), "Thermoelasticity of initially stressed bodies, Asymptotic equipartition of energies", *Int. J. Eng. Sci*., **36**(1), 73-86. https://doi.org/10.1016/S0020-7225(97)00019-0.

Martone, A., Faiella, G., Antonucci, V., Giordano, M. and Zarrelli, M. (2011), "The effect of the aspect ratio of carbon nanotubes on their effective reinforcement modulus in an epoxy matrix", *Compos. Sci. Technol*., **71**(8), 1117-1123. https://doi.org/10.1016/j.compscitech.2011.04.002.

McGee, O.G., Huang, C.S. and Leissa, A.W. (1995), "Comprehensive exact solutions for free vibrations of thick annular sectorial plates with simply supported radial edges", *Int. J. Mech. Sci*., **37**(5), 537-566. https://doi.org/10.1016/0020-7403(94)00050-T.

Mizusawa, T. (1991), "Vibration of thick annular sector plates using semi-analytical methods*", J. Sound Vib*., **150**(2), 245-259. https://doi.org/10.1016/0022-460X(91)90619-U.

Montazeri, A., Javadpour, J., Khavandi, A., Tcharkhtchi, A. and Mohajeri, A. (2010), "Mechanical properties of multi-walled carbon nanotube/epoxy composites", *Mater. Des.*, **31**, 4202-4208. https://doi.org/10.1016/j.matdes.2010.04.018.

Moradi-Dastjerdi, R. and Momeni-Khabisi, H. (2016), "Dynamic analysis of functionally graded nanocomposite plates reinforced by wavy carbon nanotube" *Steel Compos. Struct*., **22**(2). https://doi.org/10.12989/scs.2016.22.2.277.

Mukhopadhyay, M. (1979), "A semi-analytic solution for free vibration of annular sector plates", *J. Sound Vib*., **63**(1), 87-95. https://doi.org/10.1016/0022-460X(79)90379-1.

Mukhopadhyay, M. (1982), "Free vibration of annular sector plates with edges possessing different degrees of rotational restraints", *J. Sound Vib*., **80**(2), 275-279. https://doi.org/10.1016/0022-460X(82)90196-1.

Nie, G.J. and Zhong, Z. (2008), "Vibration analysis of functionally graded annular sectorial plates with simply supported radial edges", *Compos. Struct*., **84**(2), 167-176. https://doi.org/10.1016/j.compstruct.2007.07.003.

Park, W.T., Han, S.C., Jung, W.Y. and Lee, W.H. (2016), "Dynamic instability analysis for S-FGM plates embedded in Pasternak elastic medium using the modified couple stress theory", *Steel Compos. Struct*., **22**(6), 1239-1259. https://doi.org/10.12989/scs.2016.22.6.1239.

Pelletier Jacob, L. and Vel Senthil,S. (2006), "An exact solution for the steady state thermo elastic response of functionally graded orthotropic cylindrical shells", *Int. J. Solid Struct.*, **43**, 1131-1158. https://doi.org/10.1016/j.ijsolstr.2005.03.079.

Ramaiah, G.K. and Vijayakumar, K. (1974), "Natural frequencies of circumferentially truncated sector plates with simply supported straight edges", *J. Sound Vib*., **34**(1), 53-61. https://doi.org/10.1016/S0022-460X(74)80354-8.

Ramakris, R. and Kunukkas, V.X. (1973), "Free vibration of annular sector plates", *J. Sound Vib*., **30**(1), 127-129. https://doi.org/10.1016/0022-460X(83)90546-1.

Reddy J.N. (2013), "An Introduction to Continuum Mechanics", Second Edition, Cambridge University Press.

Seok, J.W. and Tiersten, H.F. (2004), "Free vibrations of annular sector cantilever plates part 1:out-of-plane motion", *J. Sound Vib*., **271**(3-5), 757-772. https://doi.org/10.1016/S0022-460X(03)00414-0.

Sharma, A., Sharda, H.B. and Nath, Y. (2005a), "Stability and vibration of Mindlin sector plates: an analytical approach", *AIAA J*., **43**(5), 1109-1116. https://doi.org/10.2514/1.4683.

Sharma, A., Sharda, H.B. and Nath, Y. (2005b), "Stability and vibration of thick laminated composite sector plates", *J. Sound Vib*., **287**(1-2), 1-23. https://doi.org/10.1016/j.jsv.2004.10.030.

Srinivasan, R.S. and Thiruvenkatachari, V. (1983), "Free vibration of annular sector plates by an integral equation technique", *J.*

Sound Vib., **89**(3), 425-432.
Srinivasan, R.S. and Thiruvenkatachari, V. (1986), "Free vibration analysis of laminated annular sector plates", *J. Sound Vib*., **109**(1), 89-96. https://doi.org/10.1016/0022-460X(83)90546-1.
Swaminadham, M., Danielski, J. and Mahrenholtz, O. (1984), "Free vibration analysis of annular sector plates by holographic experiments", *J. Sound Vib*., **95**(3), 333-340. https://doi.org/10.1016/0022-460X(83)90546-1.
Tahouneh, V. (2016), "Using an equivalent continuum model for 3D dynamic analysis of nanocomposite plates", *Steel and Composite Structures, An Int'l Journal*, **20**(3), 623-649. https://doi.org/10.12989/scs.2016.20.3.623.
Tahouneh, V. (2017), "The effect of carbon nanotubes agglomeration on vibrational response of thick functionally graded sandwich plates", *Steel and Composite Structures, An Int'l Journal*, **24**(6), 711-726. https://doi.org/10.12989/scs.2017.24.6.711.
Tornabene, F., Bacciocchi, M., Fantuzzi, N. and Reddy, J.N. (2018), "Multiscale Approach for Three-Phase CNT/Polymer/Fiber Laminated Nanocomposite Structures", *Polymer Composites*, In Press, DOI: 10.1002/pc.24520.
Tornabene, F., Fantuzzi, N., Ubertini, F. and Viola, E. (2015), "Strong Formulation Finite Element Method Based on Differential Quadrature: A Survey", Appl. Mech. Rev., **67**(2), 1-55. https://doi.org/10.1115/1.4028859.
Tornabene, F., Fantuzzi, N., Bacciocchi, M. (2019), "Refined shear deformation theories for laminated composite arches and beams with variable thickness: Natural frequency analysis", *Eng. Anal. Bound. Elem*., **100**, 24-47. https://doi.org/10.1016/j.enganabound.2017.07.029.
Tornabene, F., Fantuzzi, N., Bacciocchi, M. (2017), "Foam core composite sandwich plates and shells with variable stiffness: Effect of the curvilinear fiber path on the modal response", *J. Sandw. Struct. Mater*., **21**(1), 320-365. https://doi.org/10.1177/1099636217693623.
Wagner, H.D., Lourie, O. and Feldman, Y. (1997), "Stress-induced fragmentation of multiwall carbon nanotubes in a polymer matrix", *Appl. Phys. Lett*., **72**(2), 188-190. https://doi.org/10.1063/1.120680.
Wu, C.P. and Liu, Y.C. (2016), "A state space meshless method for the 3D analysis of FGM axisymmetric circular plates", *Steel and Composite Structures, An Int'l Journal*, **22**(1), 161-182. https://doi.org/10.12989/scs.2016.22.1.161.
Xiang, Y., Liew, K.M. and Kitipornchai, S. (1993), "Transverse vibration of thick annular sector plates*", J. of Eng. Mech. ASCE*, **119**(8), 1579-1599. https://doi.org/10.1061/(ASCE)07339399(1993)119:8(1579).
Xu, W., Wang, L., Jiang, J. (2016), "Strain Gradient Finite Element Analysis on the Vibration of Double-Layered Graphene Sheets", *International Journal of Computational Methods*, **13**(3). https://doi.org/10.1142/S0219876216500110.
Yeh, M.K., Tai, N.H. and Liu, J.H. (2006), "Mechanical behavior of phenolic-based composites reinforced with multi-walled carbon nanotubes", *Carbon*, **44**(1), 1-9. https://doi.org/10.1016/j.carbon.2005.07.005.
Zhang, Y., Wang, L. (2018), "Thermally stimulated nonlinear vibration of rectangular single-layered black phosphorus", Journal of Applied Physics, **124**(13), 10.1063/1.5047584. https://doi.org/10.1063/1.5047584.
Zhou, D., Lo, S.H. and Cheung, Y.K. (2009), "3-D vibration analysis of annular sector plates using the Chebyshev-Ritz method", *J.Sound Vib.*, **320**(1-2), 421-437. https://doi.org/10.1016/j.jsv.2008.08.001.
Zhu, X.H. and Meng, Z.Y. (1995), "Operational principle fabrication and displacement characteristics of a functionally gradient piezoelectricceramic actuator", *Sens. Actuators*, **48**(3), 169-176. https://doi.org/10.1016/0924-4247(95)00996-5.

CC

Appendix

In Generalized Differential Quadrature Method (GDQM), the *n*th order partial derivative of a continuous function $f(x,z)$ with respect to x at a given point x_i can be approximated as a linear summation of weighted function values at all the discrete points in the domain of *x*, that is

$$\frac{\partial^n f_{(x_i,z)}}{\partial x^n} = \sum_{k=1}^{N} c_{ik}^n f_{(x_{ik},z)} \quad (i=1,2,...,N, n=1,2,...,N-1) \tag{1}$$

Where *N* is the number of sampling points and c_{ij}^n is the x^i dependent weight coefficient. To determine the weighting coefficients c_{ij}^n, the Lagrange interpolation basic functions are used as the test functions, and explicit formulas for computing these weighting coefficients can be obtained as (Bert and Malik 1996)

$$c_{ij}^{(1)} = \frac{M^{(1)}(x_i)}{(x_i - x_j)M^{(1)}(x_j)}, i, j = 1,2,...,N, i \neq j \tag{2}$$

where

$$M^{(1)}(x_i) = \prod_{j=1, i\neq j}^{N} (x_i - x_j) \tag{3}$$

and for higher order derivatives, one can use the following relations iteratively

$$c_{ij}^{(n)} = n(c_{ii}^{(n-1)} c_{ij}^{1} - \frac{c_{ij}^{(n-1)}}{(x_i - x_j)}), \quad i, j = 1,2,...,N, \tag{4}$$

$$i \neq j, n = 2,3,...,N-1$$

$$c_{ii}^{(n)} = -\sum_{j=1, i\neq j}^{N} c_{ij}^{(n)} \quad i = 1,2,...,N, \quad n = 1,2,...,N-1 \tag{5}$$

A simple and natural choice of the grid distribution is the uniform grid-spacing rule. However, it was found that nonuniform grid-spacing yields result with better accuracy. Hence, in this work, the Chebyshev-Gauss-Lobatto quadrature points are used

$$x_i = \frac{1}{2}(1 - \cos(\frac{i-1}{N-1}\pi)) \quad i = 1,2,...,N \tag{6}$$